Influence of Co bilayers and trilayers on the plasmon-driven light emission from Cu(111) in a scanning tunneling microscope

Kevin Edelmann,[1,2,*] Lars Wilmes,[1] Vibhuti Rai,[1] Lukas Gerhard,[1] Liang Yang,[1,3] Martin Wegener,[1,3] Taavi Repän,[1] Carsten Rockstuhl,[1,4] and Wulf Wulfhekel[1,2]

[1]*Institute of Nanotechnology, Karlsruhe Institute of Technology (KIT), D-76344 Eggenstein-Leopoldshafen, Germany*

[2]*Physikalisches Institut, Karlsruhe Institute of Technology (KIT), D-76131 Karlsruhe, Germany*

[3]*Institute of Applied Physics, Karlsruhe Institute of Technology (KIT), D-76131 Karlsruhe, Germany*

[4]*Institut für Theoretische Festkörperphysik, Karlsruhe Institute of Technology (KIT), D-76131 Karlsruhe, Germany*

(Received 4 November 2019; revised manuscript received 27 February 2020; accepted 16 April 2020; published 5 May 2020)

Light emission from the gap cavity formed by the tip of a scanning tunneling microscope (STM) and a flat metallic sample allows us to probe the dielectric response of metals at the atomic scale and presents a way to distinguish between different materials. The excitation mechanism of the charge carrier oscillations, which ultimately decay into light, is linked to inelastic electron tunneling as opposed to the mostly semiclassical picture of the electromagnetic resonance of the gap cavity. Thus, the observed light emission does not only reflect the electromagnetic resonance of the cavity but also involves the electronic density of states. In this paper, we compare light emission from Cu(111) and Co nanoislands on Cu(111). We find a strong intensity contrast but almost no alteration of the resonance wavelength except close to step edges. Our results show that the light emission from the STM junction is highly sensitive to a few atomic layers of alien material mostly due to the dielectric properties of the layer.

DOI: 10.1103/PhysRevB.101.205405

I. INTRODUCTION

Collecting and investigating the light emitted from the tunneling junction of a scanning tunneling microscope (STM), commonly referred to as STM-induced luminescence (STML), provides a unique opportunity to probe the optical response of a nanoscopic surface area. When probing clean metal surfaces, localized plasmon-polaritons are excited within the gap between the sample and the tip by inelastic electron tunneling (IET) and partly decay into the far field [1,2]. The means of interaction between the tip and the sample is provided by the enhancement of the electric field at the very apex, so only charge carriers in a tiny radius around the apex participate in the collective oscillation, provided that a sharp tip is used [3,4]. Combined with the possibility to precisely position the STM tip, this technique offers unmatched spatial resolution and has provided deep insights into the electromagnetic coupling of electrodes at the atomic scale [5]. One specific prospect of STML is that it could provide chemical identification by spectroscopically resolving the collected light, since the local dielectric function of the sample affects the light emission. Indeed, Downes *et al.* managed to distinguish between large, spatially separated gold and copper clusters on the same sample [6]. When dealing with clean metals, such an endeavor is, however, greatly complicated by two important factors. First, the large contribution of the tip shape to the plasmonic resonance is badly controlled. In practice, STML spectra taken on the same sample material vary greatly in intensity and spectral composition when using different tips, such that it is not possible to find simple fingerprint signatures that could be used to identify a material by its light emission. This also means that STML experiments need to be performed in a comparative fashion while making sure that the tip does not change in between measurements, which is feasible if the measurements are performed on the same sample.

The other complicating factor is the energy dependence of the IET probability, which modifies the light emission but is hard to assess. After all, the emitted light in STML is the only accessible measure of this inelastic fraction of the tunneling current but carries information about both the plasmonic resonance—the classical electromagnetic property of the gap cavity consisting of the tip and the sample—and the inelastic transition probability. To what extent an observed variation of the light emission on different materials is to be attributed to either of those properties is difficult to answer and is the subject of this paper.

In this paper, we explore how far STML allows us to distinguish between two different metals, even if only a few atomic layers of alien material are present in the junction, and to what extent the change on the electromagnetic environment is responsible for the observed contrast in comparison to changes to the inelastic channel. Heteroepitaxial systems which have been investigated in STML experiments, so far, always comprised a metal in conjunction with a dielectric. Either a dielectric was used to support noble-metal grains [6–11] such that the metallic grains could be investigated

*kevin.edelmann@kit.edu

individually or noble-metal surfaces were covered with an insulating material to support molecules [12,13]. Here, we present a STML study of a heteroepitaxial system in which both constituents are metallic. In particular, Co on Cu(111) was chosen as a material system because of its well-studied growth mode, leading to a coexistence of multilayer nanoislands of different thicknesses with the bare substrate. That way, a higher variation of the material properties within the tunneling junction can be achieved as compared to systems with layer-by-layer growth. This intrinsic multilayer growth also leads to atomic steps of heights between one to four atomic layers, which allows us to determine how the emission intensity and peak wavelength observed close to step edges scale with the step height.

II. EXPERIMENT

A Cu(111) single crystal was cleaned by repeated cycles of Ar^+ ion sputtering and subsequent annealing at about 550 °C in ultrahigh vacuum conditions followed by room-temperature deposition of Co from a thermal evaporation source. To minimize the well-known intermixing of the two metals at room temperature, the sample was then transferred *in situ* into the cryogenic STM within two minutes [14,15]. To collect the emitted light from the tunneling junction, a homemade STM was used, which is described elsewhere [16]. The integrated mirror tip which was used for this experiment has been coated with approximately 60 nm of silver on the tip side. The following STML measurements were performed at 4.4 K, and the experiment shown here was performed in the constant current mode, i.e., the tunneling current was 1.5 nA across the whole investigated area at a sample bias of 2.4 V. The resolution of the optical spectrometer was about 8 nm because of its input slit width.

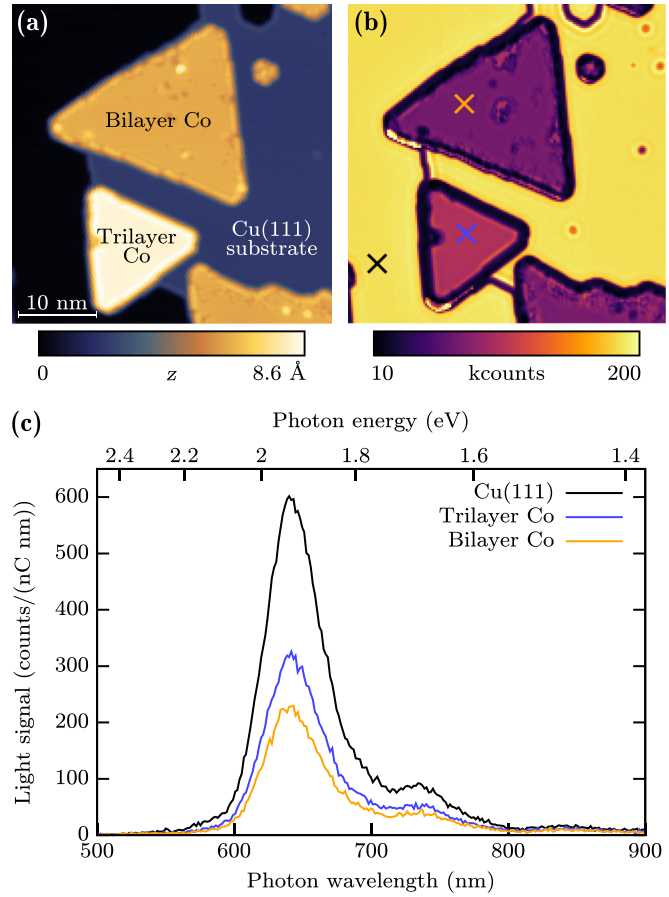

FIG. 1. (a) STM overview of the area where the photon map was recorded. (b) Map of the total photon counts. The crosses indicate where example spectra of the full wavelength range were extracted and displayed in (c).

III. RESULTS AND DISCUSSION

Figure 1(a) shows an STM topography of the investigated area, featuring mainly two individual triangular Co nanoislands much like previous studies [17–20]. The top island has an apparent height of 3.9 Å and is identified as a bilayer island [17]. It features a faulted stacking as determined by the direction of the triangle [17,18]. The top island also comprises a circumferential decoration, which, following the interpretation of Vu and Morgenstern [15], consists of Cu atoms. Apart from this, small smudges are visible on its top, which are identified as adsorbed contaminants as they could be moved with the STM tip. The bottom island is unfaulted and of trilayer height imaged 6.0 Å above the substrate. Both islands are located at the edge of a large vacancy in the Cu(111) substrate, which indicates some intermixing between the Co and Cu during sample preparation. Also, because the intermixing is known to occur first at Co islands growing at the substrate step edges [19,21], we expect only little or no intermixing within the islands presented in Fig. 1(a), which have nucleated on a Cu(111) terrace.

At the frame shown in Fig. 1(a), a so-called photon map was recorded. This means that an electroluminescence spectrum was recorded on each point while the STM tip was moved along a grid of 159 × 160 points. The exposure time of the spectrometer was 3 s for each point at a constant tunneling current of 1.5 nA. Figure 1(c) shows three representative spectra obtained from the Cu(111) substrate and both nanoislands. From these, it is already apparent that the general shape of the spectrum hardly changes when placing the tip above the Co islands, but the intensity very much does. This lateral variation is demonstrated in Fig. 1(b), in which the intensity was integrated over the entire optical spectrum for each point of the grid.

As apparent from the lack of any gradual changes or discontinuities in the photon map in Fig. 1(b), the light emission properties of the gap cavity as well as the collection efficiency of the instrument remained unchanged during the almost 30-hours-long experiment. This is essential to directly compare emission spectra which were obtained from different locations on the surface.

In the following, three different effects observed in the photon map will be discussed. First, we present how the light emission is affected by the step edges on the sample. From this, we can deduct the optical resolution—in the sense of the radius of the charge oscillation around the apex—that was achieved during this experiment, which is otherwise difficult to assess. Then, we discuss the appearance of interference patterns of the electronic surface states to demonstrate the

importance of the IET probability to the luminescence. Finally, we address the overall intensity contrast between the Cu(111) substrate and the Co islands and discuss the influence of the Co layer with respect to the optical properties of the junction based on classical full-wave optical simulations.

A. Step-edge effect

In Fig. 1(b), it can already be seen by the dark rims around islands and substrate steps that the photon emission is significantly reduced when the STM tip is placed near a step edge. Such a reduced intensity at step edges has already been observed on other closely packed noble metal surfaces like Au(111) [22], Au(110) [23], Cu(111) [24], and Ag(111) [4,25,26], whereas on Au(110), enhanced emission was observed at step edges [5,27]. The effect was finally attributed by Hoffmann *et al.* [5] to the local density of states (LDOS) at the step edge. There, a one-dimensional electronic state is formed due to electrons being trapped in their own image potential [28], resulting in a modified LDOS compared to the terrace area. In particular, this trapping leads to fewer available final states for IET on many noble metal surfaces, so gap plasmons are less likely to be excited.

It is also known that the gap plasmon is slightly shifted in energy as soon as the STM tip is placed close to a step edge. This was attributed by Aizpurua *et al.* [4] to a change of the electromagnetic properties of the gap cavity formed by the STM tip and the sample. The reasoning for this is sketched in Fig. 2(b). The highly confined tunneling current $\vec{j}$ determines the vertical tip position. The electric field $\vec{E}(t)$ of the gap plasmon is, however, less confined and may stretch over a nearby step edge and experience an average increase of the gap width when the tip is on the upper terrace. Analogously, when the tip is placed at the lower terrace close to the edge, the averaged gap as experienced by the plasmon is decreased. As the resonance energy of the gap scales with the gap width [3], approaching and passing over a descending step edge results in a blueshift at the upper terrace followed by a redshift at the lower one.

By determining the peak energy for every pixel of the photon map, we could reproduce this effect. The recorded spectra at every tip position were corrected for the detector response and fitted with an appropriate function. Then, the fitted main peak energy was plotted as a map in Fig. 2(a), showing a characteristic shift toward higher energies at the upper end of every step edge, accompanied by a shift to lower energies at the bottom end. It is demonstrated here that this effect is amplified for multiatomic step edges. Within the map in Fig. 2(a), there are step edges with one, two, three, and four atomic layer heights as indicated by the arrows. In Figs. 2(c)–2(e), profiles of the vertical tip position, the peak shift relative to 1.928 eV, as well as the fitted peak intensity were extracted along the arrows in Fig. 2(a). Along the horizontal axis, these profiles were aligned such that $x = 0$ indicates the onset of significant vertical downward movement of the tip. The vertical tip position in the upper panel was offset for clarity, such that the middle of the step is at $\Delta z = 0$ for all profiles.

Directly in front of the edge, a small protrusion can be seen in all topography profiles, indicating the edge states.

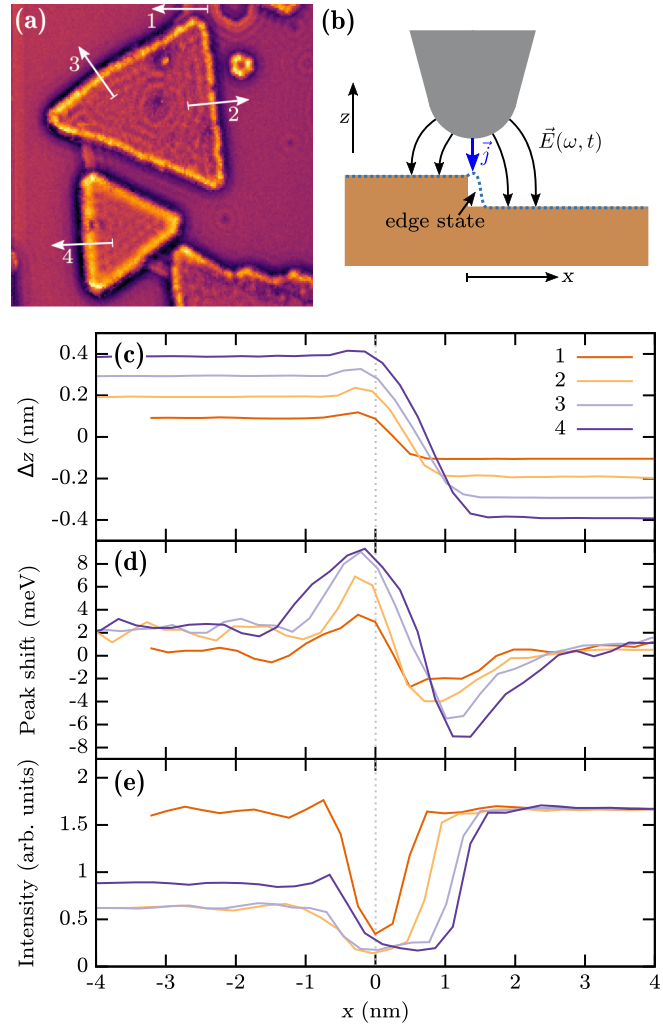

FIG. 2. Change of the cavity resonance and emitted light intensity as the STM tip is moved across vertical steps of different heights. (a) Map of the fitted main peak energy, with color scale ranging from 1.92 (dark) to 1.94 eV (bright). The arrows indicate where the profiles of vertical tip displacement, fitted peak energy, and fitted peak intensity in (c), (d), and (e) were extracted, respectively. These profiles were averaged over six adjacent lines of measurement points. The height of the steps in atomic layers is given in the key in (c). (b) Model of the gap cavity in the presence of a step edge. The dotted line represents how a step edge is typically imaged in STM due to the presence of an image state.

Due to the curvature of the tip, higher steps are imaged wider so the lower terrace is reached at higher distances x. The progression from blueshift to redshift upon passing the step edge is reproduced in Fig. 2(d). It is evident how these spectral shifts are amplified when probing higher steps, corroborating the interpretation of geometrically altering the cavity. Furthermore, the scaling of the blueshifts exhibits a saturation effect, in the sense that progressively increasing the step height results in evermore smaller increases of the peak energy, up to the point where there is almost no difference between the steps of three and four atomic layers [see left side of Fig. 2(d)]. This indicates a regime in which the gap resonance is mainly defined by the terrace closer to the apex and the lower terrace contributes only marginally.

Also, the maxima of the blueshift coincide with the maxima of the tip-sample separation at the edge state for all profiles. From the distance from the step edge at which the blueshift sets in, it can be estimated that the gap plasmon was confined to a radius of approximately 1.5 nm in this experiment. This resolution is by far high enough to probe the plasmonic response of only the Cobalt nanoislands when the STM tip is placed above one, which is a prerequisite for the discussion in Sec. III C. The maxima of the redshift, in turn, are related to the position where tunneling to the lower terrace sets in, which depends on the tip curvature and the respective step height. Consequentially, the minima in Fig. 2(d) are shifted further away from the step edge for higher steps.

The suppression in the intensity profiles in Fig. 2(e), on the other hand, does not scale with the height of the step edges, which rules out major contributions of any mechanism that relies on changes in the geometry, such as the originally proposed angle between the tunneling current and the surface normal [24]. Only the profile in Fig. 2(e) which spans across the monoatomic step exhibits a higher emission intensity at the step edge compared to the other three profiles. However, this specific profile involves an upper Cu terrace, whereas all of the other probed steps consist of an upper Co terrace. Therefore, we suggest that this effect might have the same origin as the overall material contrast discussed in Sec. III C.

B. Friedel oscillations

In isochromatic maps of the photon intensity, i.e., maps showing the integrated photon counts within a certain photon wavelength range, one can observe standing wave patterns with a wavelength of approximately 1 nm. This is exemplarily shown in Fig. 3, in which two areas of interest have been extracted and are displayed with adapted color contrast. The standing waves emerge on the Cu area at step edges and surface impurities, and similarly on the islands. This is no plasmonic feature but resembles standing waves of the electronic surface state [31]. The reason why these variations of the LDOS manifest in the photon maps is that the density of available final states $\rho(E_{\mathrm{fi}})$ of the electrons after giving energy to the gap plasmon modifies the probability for IET and, therefore, the light emission intensity. So even though the inelastic tunneling current makes up only a small part of the total current, the light emission is a sensitive probe for it. In the constant current mode, the tip is positioned by the feedback loop such that the tunneling current, i.e., the LDOS in front of the sample surface at the tip position integrated over the bias voltage window, is constant [32]. The primary excitation mechanism by IET is thus proportional to the LDOS of the final state of the electron after IET.

In the following, it will be shown that the imaged oscillations in Fig. 3(a) are, in fact, Friedel oscillations of the surface state. Assuming a positive sample bias V, as was used in the presented experiment, electrons tunnel from the occupied state of the tip into unoccupied states of the sample. At that, all occupied tip states at initial energy $E_{\mathrm{in}} \geqslant E_{\mathrm{F,\,sample}} + \hbar\omega$ will additionally contribute to inelastic transitions as shown in Fig. 3(b). The IET probability of all channels with $E_{\mathrm{in}} - E_{\mathrm{fi}} = \hbar\omega$ depends on the LDOS of all involved final states in the sample, as well as the LDOS of all involved initial states in the tip, and their respective tunneling barriers. As E_{in} is not fixed due to contributions of electrons below the Fermi energy to the tunneling current, the light intensity at a certain photon energy cannot be linked to a specific energy of

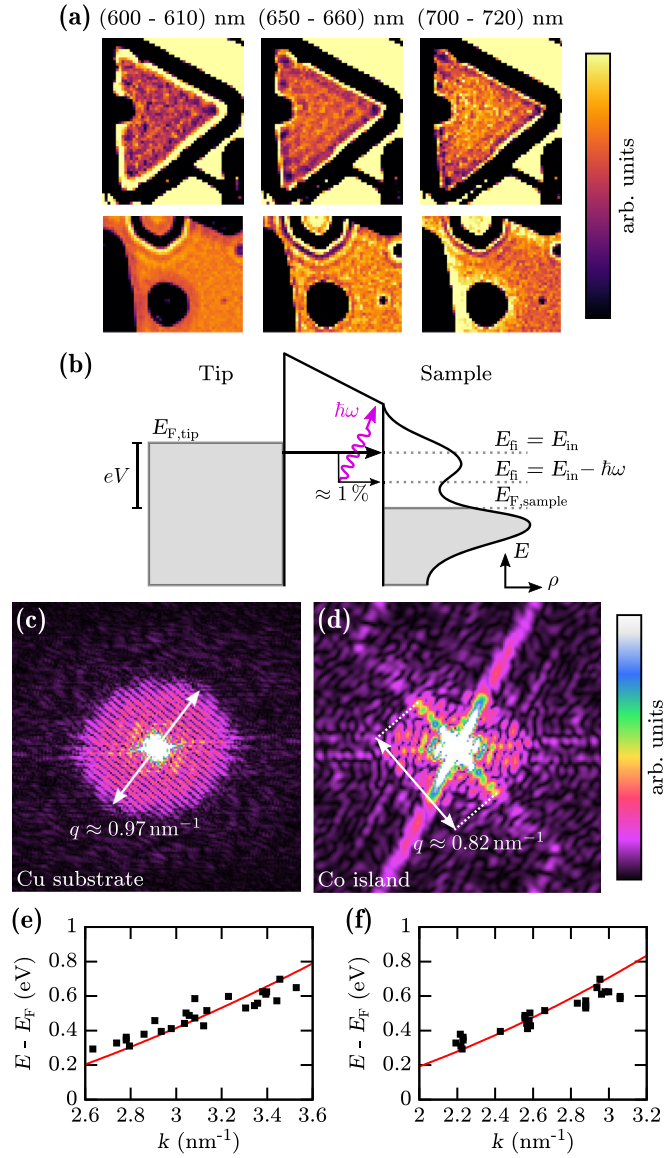

FIG. 3. Standing-wave patterns of the electronic surface state as observed in the photon map. (a) Maps of photon counts within the indicated wavelength intervals recorded on the trilayer Co island (top) and a section of the Cu(111) substrate (bottom). The false color scale was adapted to highlight the Friedel oscillations of decreasing wavelength as the photon wavelength increases. (b) Model of a single IET channel responsible for the emission of photons of a certain energy $\hbar\omega$. (c), (d) 2D Fourier transforms of the isochromatic maps (650 to 660 nm) including only the Cu(111) area and trilayer Co island, respectively. The diameter of the solid disk in (c) and the length of the line in (d) were identified as twice the inverse wavelength of the wave patterns visible in (a). (e), (f) Extracted dispersion relations for the surface state of the Cu(111) and the Co trilayer nano-island, respectively. Black squares denote data points of this work, the solid red lines represent the dispersion relations with effective mass of 0.40 [29] and 0.37 [30] for Cu and Co, respectively.

the end state. As a result, isochromatic photon maps reflect spatial variations of the LDOS of a broad range of end states, which all feature different wavelengths on the surface due to the dispersion of the surface state. When imaging different wavelength components at the same time, they dephase with increasing distance from the scatterer [33,34], which is why the observed coherence length of the intensity oscillations in Fig. 3(a) spans only a few wave cycles, even though the lifetime of the corresponding surface state is long enough at 4.4 K to decay only within several 10 nm [29]. This effect is increased further by the limited resolution of the spectrometer and the fact that photon maps were integrated over a certain photon wavelength range.

This mixture of spatial frequency components is reflected in the 2D Fourier transforms of the intensity maps, e.g., integrating from 650 to 660 nm on the Cu substrate [Fig. 3(c)] and the smaller trilayer island [Fig. 3(d)]: The point scatterers on the Cu substrate produce circular wave patterns that result in rings of different diameter in the Fourier transform and add up to a solid disk. Analogously, the standing-wave patterns on the Co island are caused by the confinement by the island edges, resulting in straight wave trains and, in the Fourier transform, a line. Now, the largest wave numbers present in the Fourier transform maps can actually be related to a specific transition, as they correspond to the highest possible final state for IET at constant tunneling bias and energy loss to the gap plasmon. As apparent from Fig. 3(b), only electrons from the Fermi edge of the tip contribute to transitions ending up at the highest possible end state, so E_{in} is known for these transitions and E_{fi} simply follows as

$$E_{\mathrm{fi}} = E_{F,\,\mathrm{sample}} + eV - \hbar\omega. \tag{1}$$

The diameter of the solid disk and the length of the solid lines in Figs. 3(c) and 3(d) yield the wave vector of the surface state at this specific E_{fi}. Consequently, each isochromatic intensity map yields one point of the dispersion relation $E(|\vec{k}|)$ of the involved surface states.

By applying this procedure to different maps which integrate over different sections of the optical spectrum, the dispersion relation can be extracted within a certain energy range and compared to the literature. For that purpose, 26 isochromatic maps were rendered, which cover the photon wavelength range from 590 to 740 nm. The interval between each map is 5 nm up to 700 nm and 10 nm from then on, and each map integrates over a photon wavelength range of 10 nm. The inverse of the wavelength $q = \lambda^{-1}$ of the spatial oscillations of the LDOS can be directly extracted from the Fourier-transformed photon map as the radius of the disk or half of the line's length in Figs. 3(c) and 3(d), respectively. As the variations in the LDOS are caused by the interference of the surface state electrons and are proportional to the square of the wave function $|\Psi|^2$, the wave vector k of the surface state is $k = \pi q$.

In Figs. 3(e) and 3(f), the extracted dispersions are converted into angular wave numbers k and compared with the dispersion relations reported by Pietzsch *et al.* [14] as measured by scanning tunneling spectroscopy. The bilayer island in our experiment contained too many scattering centers to develop a clear wave pattern. Instead, we compare the reference curve to the dispersion extracted from the trilayer island. This exhibits a discrete spectrum with essentially only three allowed wave numbers within the probed energy range due to the small size of the island (discrete particle-in-a-box states [31]). Apart from this detail, the values from the luminescence measurement are in plausible agreement with the reference curves for both the Cu(111) area and the Co island.

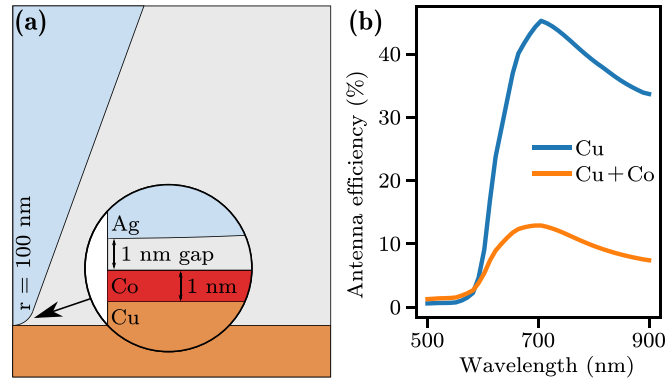

FIG. 4. (a) Geometry of the numerical simulation of the tip in front of the sample. (b) Antenna efficiency as function of wave length for a Cu sample, 1 nm of vacuum and an Ag tip (blue) and the same with an additional layer of 1 nm Co in the junction (orange).

It is noteworthy that Schull *et al.* [31] have already observed Friedel oscillations in light intensity maps, and they have already established a technique to compare the standing waves in intensity maps with the dispersion of the surface state. Their approach, however, relies on a fitting procedure, which is only successful for very good signal-to-noise ratios and a tunneling bias which is only slightly higher than the probed photon range. That way, only electrons close to the Fermi edge can participate in the relevant IET channels, and the mixing of spatial wavelengths in the intensity maps is reduced.

C. Intensity contrast

As already apparent from Figs. 1(b) and 1(c), the emission intensity obtained from the Co nanoislands is significantly lower compared to the luminescence from the bare Cu(111) surface, while the overall shape and peak position are virtually the same, i.e., the photon emission is highly sensitive to a few monolayers of alien material. In the following, it will be discussed how far this intensity contrast is to be attributed to a variation of the electromagnetic and electronic properties of the materials.

As STM does not offer a direct access to the optical properties of the junction, we performed full-wave optical simulations of the tip-substrate situation using the three-dimensional finite-element-based Maxwell solver JCMsuite to appreciate the experimental results. A cross section of the considered geometry is shown in Fig. 4(a). It qualitatively corresponds in its geometrical feature to the experimental situation. The radius of curvature of the tip-apex was 100 nm, i.e., in close proximity to the actual tunneling junction, the interface is considered as nearly flat. In the simulation, we model all parts in a continuum approximation with a semi-infinite Cu substrate on

top of which a thin (1 nm) Co layer is optionally placed and the apex of the Ag tip is positioned 1 nm above the surface. Based on prior work [35], we consider the emission from a vertical dipole that is positioned in the center of the junction. In the low pumping regime, the overall amount of the emission is proportional to pump rate and the antenna efficiency of the system [36]. The antenna efficiency is the fraction of the overall extracted energy from the emitter radiated into the far field. The remaining energy is dissipated in either substrate, optional Co layer, or the tip. Optical properties of the metals in the simulations where taken form Johnson and Christy [37]. In the pumping rate, the actual excitation efficiency is condensed that mostly relates to the LDOS and IET. In the simulations, we keep it constant to discuss only the impact of the layered material purely from an optical perspective.

Figure 4(b) shows the antenna efficiency for the situation without (blue) and with Co layer (orange). The strong decline in antenna efficiency at wavelengths below 600 nm for both cases is assigned to the onset of a rather large imaginary part in Cu below that wavelength (giving Cu its red color upon visual inspection). Cu becomes much more absorptive in this spectral region which in turn denies to extract radiation into the far field. A control simulation with a Cu tip instead of a Ag tip showed essentially the same behavior (not shown) but with a slightly lower overall antenna efficiency. Thus, choosing silver as the tip material does have at most a minor effect. Instead, the properties of the junction are rather dominated by the Cu substrate, as the basic functional dependency can be explained with the onset of the imaginary part of Cu below 600 nm. After a sudden increase of the antenna efficiency at 600 nm, the antenna efficiency slowly drops at longer wavelengths. The overall dispersion of the antenna efficiency deviates from the experimental spectra. However, the exact shape of the spectrum is strongly influenced by the actual geometrical shape of the tip, which is not under control in the experiments. As already mentioned initially, different tips would allow us to measure different spectra. Thus, deviation between theory and experiment at longer wavelengths are expected.

However, and most relevant to the present study, the antenna efficiency is significantly reduced by the presence of the rather thin Co layer. Co is a bad metal that enhances dissipation and allows us to couple out less radiation to the far field. Moreover, at wavelengths slightly longer than 600 nm up to to the shown wavelength of 900 nm, no dispersive features are introduced by the Co film from which one has to expect a modification of the spectrally resolved characteristics of the emission, i.e., mainly a scaling of the magnitude is expected to happen without inducing new peaks in the spectral composition. This is in good agreement with the experimental observation and illustrates that damping due to even thin layers of bad metals largely affect the light emission from STM junctions.

The changes of the optical properties of the junction qualitatively explain the reduced emission of photons on Co islands. On top of this, the LDOS and the branching ratio for IET will also play a role as it determines the pump rate. As evidenced by the bilayer Co islands appearing darker in the photon maps than the trilayer islands, these intensity variations cannot be due to the dissipation in the optical frequency range. Instead, it indicates differences due to the primary excitation process. We, however, cannot quantify exactly the impact of the IET efficiency as, experimentally, it is impossible to alter the electromagnetic properties of materials and their electronic structure in these few monolayer films independently.

IV. CONCLUSION

We have presented high-resolution STML photon maps of a heteroepitaxial, metallic system with excellent photon statistics. We systematically investigated the light emission close to step edges of different heights regarding the plasmonic resonance shift and emission intensity. Our findings corroborate earlier theories which state that the peak shift is a result of geometrically altering the gap cavity, whereas the intensity drop is due to a reduced IET probability when tunneling into the one-dimensional edge state. We then used the observation of electronic standing waves in emission maps to demonstrate the importance of the IET probability to the luminescence, while even thin layers of a bad metal significantly suppress light emission due to damping but without changing the spectral shape. Apart from small resonance shifts close to the step edges, the overall shape of the emission spectra was found to be unaffected by the different materials and is dominated in our case by the optical properties of the Cu substrate.

ACKNOWLEDGMENTS

We thank Martin Schumann for his help with manufacturing the mirror tip which was used for this experiment and the referee for stimulation to carry out numerical simulations. This work was supported by the Helmholtz program Science and Technology of Nanosystems (STN), by the Deutsche Forschungsgemeinschaft (DFG, German Research Foundation) under Germany's Excellence Strategy via the Excellence Cluster 3D Matter Made to Order (No. EXC-2082/1-390761711), by the Carl Zeiss Foundation through the Carl-Zeiss-Focus@HEiKA and the Volkswagen Foundation. V.R. gratefully acknowledges funding by the Deutsche Akademische Austauschdienst (DAAD). The authors are grateful to the company JCMwave for their free provision of the FEM Maxwell solver JCMsuite with which the simulations have been performed.

[1] R. Berndt, J. K. Gimzewski, and P. Johansson, Inelastic Tunneling Excitation of Tip-Induced Plasmon Modes on Noble-Metal Surfaces, Phys. Rev. Lett. **67**, 3796 (1991).

[2] R. Berndt and J. K. Gimzewski, The role of proximity plasmon modes on noble metal surfaces in scanning tunneling microscopy, Surf. Sci. **269**, 556 (1992).

[3] R. W. Rendell and D. J. Scalapino, Surface plasmons confined by microstructures on tunnel junctions, Phys. Rev. B **24**, 3276 (1981).

[4] J. Aizpurua, G. Hoffmann, S. P. Apell, and R. Berndt, Electromagnetic Coupling on an Atomic Scale, Phys. Rev. Lett. **89**, 156803 (2002).

[5] G. Hoffmann, T. Maroutian, and R. Berndt, Color View of Atomic Highs and Lows in Tunneling Induced Light Emission, Phys. Rev. Lett. **93**, 076102 (2004).

[6] A. Downes, P. Guaino, and P. Dumas, Color mapping by scanning tunneling microscopy: Chemical analysis of metal surfaces, Appl. Phys. Lett. **80**, 380 (2002).

[7] P. Dumas, C. Syrykh, I. V. Makarenko, and F. Salvan, STM-induced light emission of supported silver nanocrystallites, EPL **40**, 447 (1997).

[8] N. Nilius, N. Ernst, and H.-J. Freund, Photon Emission Spectroscopy of Individual Oxide-Supported Silver Clusters in a Scanning Tunneling Microscope, Phys. Rev. Lett. **84**, 3994 (2000).

[9] N. Nilius, Experiments on individual alumina-supported adatoms and clusters, Prog. Surf. Sci. **67**, 99 (2001).

[10] N. Nilius, N. Ernst, and H.-J. Freund, Tip influence on plasmon excitations in single gold particles in an STM, Phys. Rev. B **65**, 115421 (2002).

[11] P. Myrach, N. Nilius, and H.-J. Freund, Photon mapping of individual Ag particles on MgO/Mo(001), Phys. Rev. B **83**, 035416 (2011).

[12] X. H. Qiu, G. V. Nazin, and W. Ho, Vibrationally resolved fluorescence excited with submolecular precision, Science **299**, 542 (2003).

[13] E. Ćavar, M.-C. Blüm, M. Pivetta, F. Patthey, M. Chergui, and W.-D. Schneider, Fluorescence and Phosphorescence from Individual C_{60} Molecules Excited by Local Electron Tunneling, Phys. Rev. Lett. **95**, 196102 (2005).

[14] O. Pietzsch, S. Okatov, A. Kubetzka, M. Bode, S. Heinze, A. Lichtenstein, and R. Wiesendanger, Spin-Resolved Electronic Structure of Nanoscale Cobalt Islands on Cu(111), Phys. Rev. Lett. **96**, 237203 (2006).

[15] Q. H. Vu and K. Morgenstern, Upward mass transport and alloying during the growth of Co on Cu(111), Phys. Rev. B **95**, 125423 (2017).

[16] K. Edelmann, L. Gerhard, M. Winkler, L. Wilmes, V. Rai, M. Schumann, C. Kern, M. Meyer, M. Wegener, and W. Wulfhekel, Light collection from a low-temperature scanning tunneling microscope using integrated mirror tips fabricated by direct laser writing, Rev. Sci. Instr. **89**, 123107 (2018).

[17] J. de la Figuera, J. E. Prieto, C. Ocal, and R. Miranda, Scanning-tunneling-microscopy study of the growth of cobalt on Cu(111), Phys. Rev. B **47**, 13043 (1993).

[18] A. L. Vazquez de Parga, F. J. García-Vidal, and R. Miranda, Detecting Electronic States at Stacking Faults in Magnetic Thin Films by Tunneling Spectroscopy, Phys. Rev. Lett. **85**, 4365 (2000).

[19] O. Pietzsch, A. Kubetzka, M. Bode, and R. Wiesendanger, Spin-Polarized Scanning Tunneling Spectroscopy of Nanoscale Cobalt Islands on Cu(111), Phys. Rev. Lett. **92**, 057202 (2004).

[20] S. Schmaus, A. Bagrets, Y. Nahas, T. K. Yamada, A. Bork, M. Bowen, E. Beaurepaire, F. Evers, and W. Wulfhekel, Giant magnetoresistance through a single molecule, Nature Nanotechnology **6**, 185 (2011).

[21] J. de la Figuera, J. E. Prieto, G. Kostka, S. Müller, C. Ocal, R. Miranda, and K. Heinz, Crystallography and morphology of the early stages of the growth of by LEED and STM, Surf. Sci. **349**, L139 (1996).

[22] G. Hoffmann, J. Aizpurua, P. Apell, and R. Berndt, Influence of tip geometry in light emission from the scanning tunneling microscope, Surf. Sci. **482-485**, 1159 (2001).

[23] J. G. Keizer, J. K. Garleff, and P. M. Koenraad, Simple and efficient scanning tunneling luminescence detection at low-temperature, Rev. Sci. Instrum. **80**, 123704 (2009).

[24] R. Berndt and J. K. Gimzewski, Photon emission in scanning tunneling microscopy: Interpretation of photon maps of metallic systems, Phys. Rev. B **48**, 4746 (1993).

[25] Y. Suzuki, H. Minoda, and N. Yamamoto, STM light emission from Ag/ Si(111), Surf. Sci. **438**, 297 (1999).

[26] C. Zhang, B. Gao, L. G. Chen, Q. S. Meng, H. Yang, R. Zhang, X. Tao, H. Y. Gao, Y. Liao, and Z. C. Dong, Fabrication of silver tips for scanning tunneling microscope induced luminescence, Rev. Sci. Instrum. **82**, 083101 (2011).

[27] R. Berndt, R. Gaisch, W. D. Schneider, J. K. Gimzewski, B. Reihl, R. R. Schlittler, and M. Tschudy, Atomic Resolution in Photon Emission Induced by a Scanning Tunneling Microscope, Phys. Rev. Lett. **74**, 102 (1995).

[28] L. Bartels, S. W. Hla, A. Kühnle, G. Meyer, K.-H. Rieder, and J. R. Manson, STM observations of a one-dimensional electronic edge state at steps on Cu(111), Phys. Rev. B **67**, 205416 (2003).

[29] L. Bürgi, O. Jeandupeux, H. Brune, and K. Kern, Probing Hot-Electron Dynamics at Surfaces with a Cold Scanning Tunneling Microscope, Phys. Rev. Lett. **82**, 4516 (1999).

[30] L. Diekhöner, M. A. Schneider, A. N. Baranov, V. S. Stepanyuk, P. Bruno, and K. Kern, Surface States of Cobalt Nanoislands on Cu(111), Phys. Rev. Lett. **90**, 236801 (2003).

[31] G. Schull, M. Becker, and R. Berndt, Imaging Confined Electrons with Plasmonic Light, Phys. Rev. Lett. **101**, 136801 (2008).

[32] J. Tersoff and D. R. Hamann, Theory and Application for the Scanning Tunneling Microscope, Phys. Rev. Lett. **50**, 1998 (1983).

[33] Y. Hasegawa and P. Avouris, Direct Observation of Standing Wave Formation at Surface Steps Using Scanning Tunneling Spectroscopy, Phys. Rev. Lett. **71**, 1071 (1993).

[34] P. Avouris, Real space imaging of electron scattering phenomena at metal surfaces, J. Vac. Sci. Technol. B **12**, 1447 (1994).

[35] P. Bharadwaj, A. Bouhelier, and L. Novotny, Electrical Excitation of Surface Plasmons, Phys. Rev. Lett. **106**, 226802 (2011).

[36] R. Filter, K. Słowik, J. Straubel, F. Lederer, and C. Rockstuhl, Nanoantennas for ultrabright single photon sources, Opt. Lett. **39**, 1246 (2014).

[37] P. B. Johnson and R. W. Christy, Optical constants of the noble metals, Phys. Rev. B **6**, 4370 (1972).